Evolution and Frontogenesis of an Imbalanced Flow —the Influence of Vapor Distribution and Orographic Forcing①

Wang Yunfeng (王云峰), Wu Rongsheng(伍荣生), and Pan Yinong(潘益农)

Laboratory of Mesoscale Severe Weather, Nanjing University, Nanjing 210093

(Received June 7, 1999, revised August 10, 1999)

ABSTRACT

If the initial fields are not in geostrophic balance, the adjustment and evolution will occur in the stratified fluid, and the frontogenesis will occur under suitable conditions. The evolution is studied here with a nonhydrostatic fully compressible meso–scale model (Advanced Regional Prediction System, ARPS). Four cases are designed and compared: (i) control experiment; (ii) with different initial temperature gradient; (iii) with vapor distribution; (iv) with orographic forcing. The results show that: (1) there is an inertial oscillation in the evolution of the imbalanced flow with the frequency of the local Coriolis f, and with its amplitude decreasing with time. The stationary balanced state can only be approached as it cannot be reached in the limit duration of time. The energy conversion ratio varies in the range of [0, 1 / 3]; (2) the stronger initial temperature gradient can make the final energy conversion ratio higher, and vice versa; (3) suitable vapor distribution is favorable for the frontogenesis. It will bring forward the time of the frontogenesis, strengthen the intensity of the cold front, and influence the final energy conversion ratio; (4) the orographic forcing has an evidently strengthening effect on the frontogenesis. The strengthening effect on the frontogenesis and the influence on the final energy conversion ratio depend on the relative location of the mountain to the cold front.

Key words: Evolution, Frontogenesis, Inertial oscillation, Vapor distribution and orographic forcing

1. Introduction

If the initial fields are not in geostrophic balance, the adjustment and evolution will occur in the stratified fluid, and the frontogenesis will occur under suitable conditions. This aspect was first investigated by Rossby (1938), followed by many scientists (Blumen, 1972; Gill, 1976, 1982; Van Heijst, 1985; Boss and Thompson, 1985; Ou, 1984, 1986; McWilliams, 1988; Middleton, 1987; Glendening, 1993; Blumen and Wu, 1995; Wu and Blumen, 1995; Grimshaw 1998; Blumen, 1998; etc.). In these researches, the energy conversion ratio $\gamma = \Delta E_k / \Delta E_p$ is an interesting topic, where $\Delta E_k = E_k(t) - E_k(t_0)$ and $\Delta E_p = E_p(t_0) - E_p(t)$ are the variations of the actual kinetic energy and the potential energy between the final state and the initial state respectively. The similar conclusions were obtained that γ varied in the range of [0, 1 / 2]. However, these researches were made in the two–dimensional incompressible stratified fluid, which satisfied the conservation of potential vorticity. What occurred to the three–dimensional fully compressible stratified fluid? This is one of the questions we discuss in this paper.

①This work was supported by the National Natural Science Foundation of China under grants: 49675259 and 49735180, and by the State Key Basic Program: CHERES.

Blumen and Wu (1995) and Wu and Blumen (1995) calculated the final balanced fields directly from the initial imbalanced fields, neglecting the evolution. So the details of the frontogenesis cannot be obtained in their researches. Furthermore, whether the final geostrophic balanced state will be reached or not and whether the front will form or not within the limited time are open topics for further investigation. In addition, the frontogenesis occurs as $\frac{\partial v}{\partial X} = 1$ in their researches. But according to the theoretical frame of Geostrophic Momentum Coordinates, when this equation is satisfied, the coordinate transformation has to be terminated and the following evolution cannot be studied. Blumen (1998) studied the geostrophic frontogenesis in the inviscid, two-dimensional, rotating, nonlinear fluid. His research remedied the above shortage of time-dimension in some sense, making it possible to study the evolution with time. However, his model was limited to the two-dimensional, and satisfied the limitation of the zero potential vorticity. For more complicated three-dimensional fully compressible nonlinear rotating stratified fluid, further research is necessary.

Finally, both vapor distribution and orographic forcing are very important factors for the numerical weather forecast. China faces the Pacific on the east, with the vapor abundant above the sea surface, as well as with the terrain complicated on land. It is very important to consider the influences of the two factors on the evolution of the imbalance flow. In our research the influences have been studied and compared with the control experiment, and some interesting results are obtained.

A three-dimensional non-hydrostatic meso-scale model (ARPS) is used to study the above mentioned problems. The model and the initial conditions are briefly described in Section 2. The numerical results and discussion are presented in Section 3. The conclusion is given in Section 4.

2. ARPS model description and initial field design

ARPS (Advanced Regional Prediction System) is a nonhydrostatic fully compressible storm- and meso-scale prediction model developed at the Center for Analysis and Prediction of Storms (CAPS), University of Oklahoma. Various physical processes are taken into account in the model system. The governing equations are solved in a rectangular computational space. And they are solved on a standard Arakawa *C* grid with a split-explict solution technique in which the acoustic modes are explicitly integrated with a forward-backward scheme on small time steps. The equations are discretized with fourth-order centered spatial differences and integrated on big time steps with the leapfrog scheme and a Robert-Asselin time filter. A complete description of the model, including the governing equations, initialization, boundary condition options, discretizations, and numerical solution techniques can be found in the ARPS Version 4.0 User's Guide (Ming Xue et al., 1995).

In this paper, a horizontal mesh with 83 × 83 grid points centered at 45°N and 90°E was designed. The horizontal grid size is equal to 30 km. There are 33 grid points in the vertical direction, with the computational grid size 400 m (real vertical coordinate is stretched and divided into 33 nonuniform layers). In this study, the friction is excluded, and the fluid is assumed as the open lateral boundary condition in the horizontal direction and the rigid condition at the upper and bottom boundary. The applied map projection in the model's equations is Lambert conformal true at 30°N and 60°N.

Four initial fields are designed as follows:

2.1 *Control experiment*

The initial wind fields are in rest:

$$u = 0, \qquad v = 0. \tag{1}$$

The initial temperature distribution in the horizontal direction is only dependent on latitude. That is:

$$t = A\tanh(By + y_0) + \Gamma z, \tag{2}$$

where A denotes the amplitude of temperature; B denotes the controlling parameter of the temperature gradient strength; y denotes the south–north coordinate; y_0 denotes the phase parameter, and Γ represents the vertical lapse rate. In control experiment, we take:

$$A = 15.0^\circ\mathrm{C}, \quad B = 0.3, \quad y_0 = 0.0, \quad \Gamma = -0.006^\circ\mathrm{C/m}. \tag{3}$$

Because not all imbalanced flows are favorable for the frontogenesis, the purpose taking these initial fields is to promise that the frontogenesis happen during the adjustment and evolution (Blumen and Wu, 1995; Wu and Blumen, 1995; Majid and Wu, 1998).

The initial surface pressure distribution can be expressed as:

$$p = p_0 + C\tanh(By + y_0). \tag{4}$$

Where $C = 15.0$ hPa denotes the amplitude of pressure, $p_0 = 1000$ hPa. Pressure on other levels can be calculated by hydrostatic equation, that is:

$$\frac{\partial p}{\partial z} = -\rho g = -\frac{pg}{RT}. \tag{5}$$

2.2 With different initial temperature gradient

Taking $A = 10.0^\circ$C, $B = 0.2$, other parameters are the same as those of the control experiment.

2.3 With vapor distribution

For the factor of vapor distribution, two initial fields are designed. The first is an evidently sea–land typed initial field, as follows:

$$\text{The eastern part is sea area:} \quad \mathrm{RH} = \begin{cases} 60 & 18 \leqslant k \leqslant 33 \\ 100 & 1 \leqslant k \leqslant 17, \end{cases} \tag{6}$$

$$\text{The western part is land area:} \quad \mathrm{RH} = 10, \tag{7}$$

where k denotes the vertical level number from bottom to top, RH denotes the relative humidity.

The other is a strip–like typed initial field, as follows:

$$\text{In the area } 16 \leqslant j \leqslant 18: \quad \mathrm{RH} = \begin{cases} 60 & 18 \leqslant k \leqslant 33 \\ 100 & 1 \leqslant k \leqslant 17, \end{cases} \tag{8}$$

$$\text{In other area:} \quad \mathrm{RH} = 10, \tag{9}$$

where j denotes the meridional grid number from south to north.

2.4 *With orographic effect*

The mountain profile is given as:

$$h = \frac{h_m}{[1 + (\frac{x - x_c}{a})^2 + (\frac{y - y_c}{b})^2]}, \tag{10}$$

where h_m is the maximum mountain height, a and b are the mountain half-width along x and y direction respectively, (x_c, y_c) is the central position of the maximum mountain height.

Two different initial fields are considered as follows:

$$h_m = 2 \text{ km}, \quad a = b = 200 \text{ km}, \quad x_c = y_c = 1200 \text{ km}, \tag{11}$$

which promise the cold frontogenesis happening and keeping at the down-slope side;

$$h_m = 2 \text{ km}, \quad a = b = 200 \text{ km}, \quad x_c = 1200 \text{ km}, \quad y_c = 500 \text{ km}, \tag{12}$$

which promise the cold frontogenesis happening and keeping at the up-slope side.

3. Numerical results and discussion

3.1 *Control experiment*

The initial fields of control experiment are given in Fig 1.

It shows that the isopleth crowded area exists in the temperature field and the pressure field respectively. For the temperature field, the warm area is in the south of the domain, and the cold area is in the north. For the low level, low-pressure is in the south and high-pressure is in the north; while for the high level, low-pressure is in the north, and high-pressure is in the south. Both the temperature field and the pressure field continuously vary at the interface. Because the wind fields are at rest, these initial fields are not in geostrophic balance, the adjustment and evolution will occur. In this experiment, $\frac{\partial \theta}{\partial y}$ is assumed as uniform at the vertical direction (figure not given).

Wu and Blumen (1995) pointed out that a criterion for frontogenesis is whether $\frac{\partial v}{\partial X}$ equal to 1. In our research, if the temperature gradient is continually enhancing and finally it can reach a certain value, this evolution can be regarded as the frontogenesis.

Boussinesq approximation is included in this research. The integral time-step is 24 seconds. The results at $t = 5.0$ h are given in Fig. 2.

Fig. 2a shows that the surface isothermal denseness is stronger than before and it moves toward the warm area. This is a typical adjustment-typed cold front. Fig. 2b is the surface distribution of u-v streamline. It shows that there is a strong convergence line in the frontal area. In the wide area north to the cold front there is northeast wind. And there is a strong divergence line in the north of the domain. Ahead of the cold front there is the updraft, and behind the cold front there is the downdraft. The circulation pattern is consistent with the classical frontal circulation type. Fig. 2c is the vertical distribution of temperature, which shows that the frontogenesis occurs at both the top and bottom boundaries respectively. These results are confirmed to the theoretical results of Blumen and Wu (1995). Near the surface, the isotherm is almost vertical, which is consistent with the observational fact of the front. Wang and Wu (1998) pointed out that the frontogenesis at the top boundary, which is due to the compensative effect of the mass flow, would disappear when the stratification difference between the cold area and the warm area was considered. We also verify this result through the

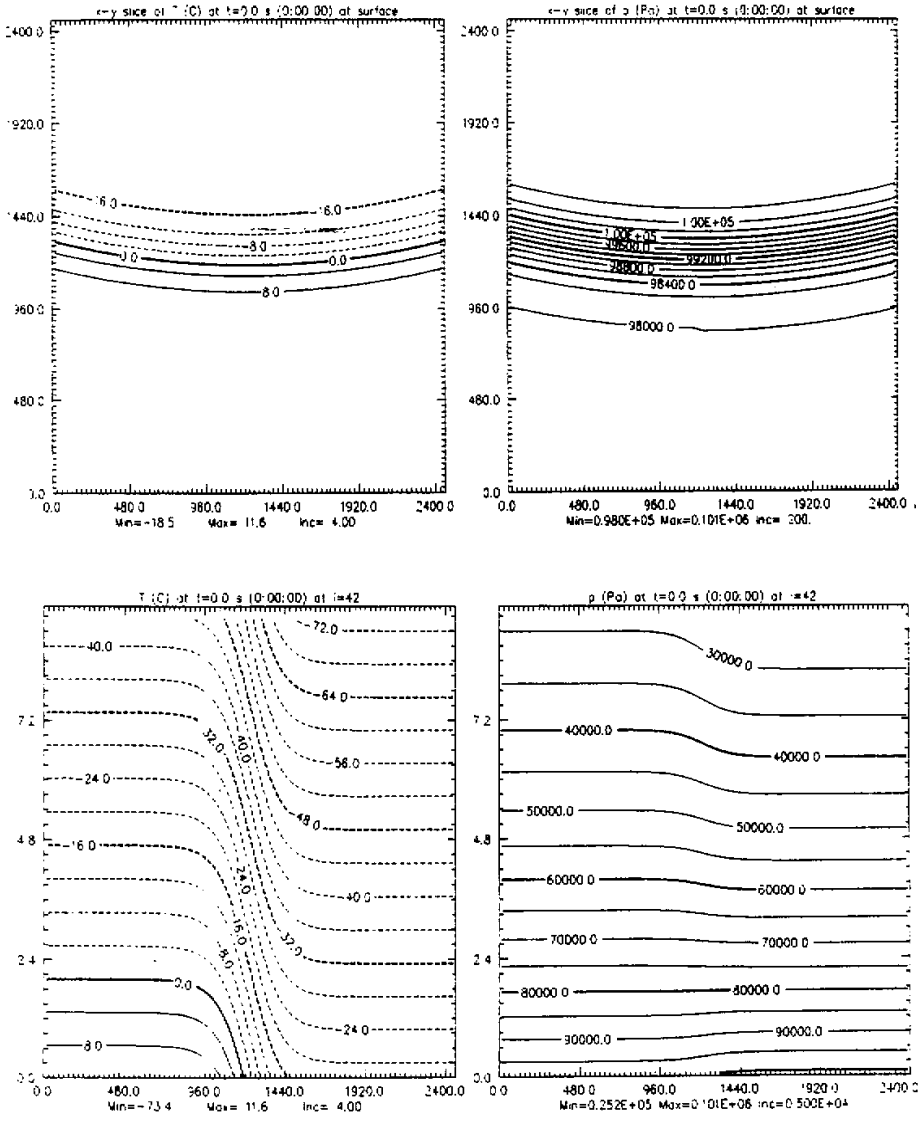

Fig. 1. The initial horizontal distributions at surface and the initial vertical distributions through the center in x direction in control experiment. (a) the horizontal distribution of initial temperature; (b) the horizontal distribution of initial pressure; (c) the vertical distribution of initial temperature; (d) the vertical distribution of initial pressure.

numerical experiment, but make no discussions in this paper for simplicity. Fig. 2d shows the vertical distribution of the vertical velocity. There is the updraft before the front, and the downdraft behind the front. In the nonlinear adjustment system, the potential vorticity is not conserved. Its strength will

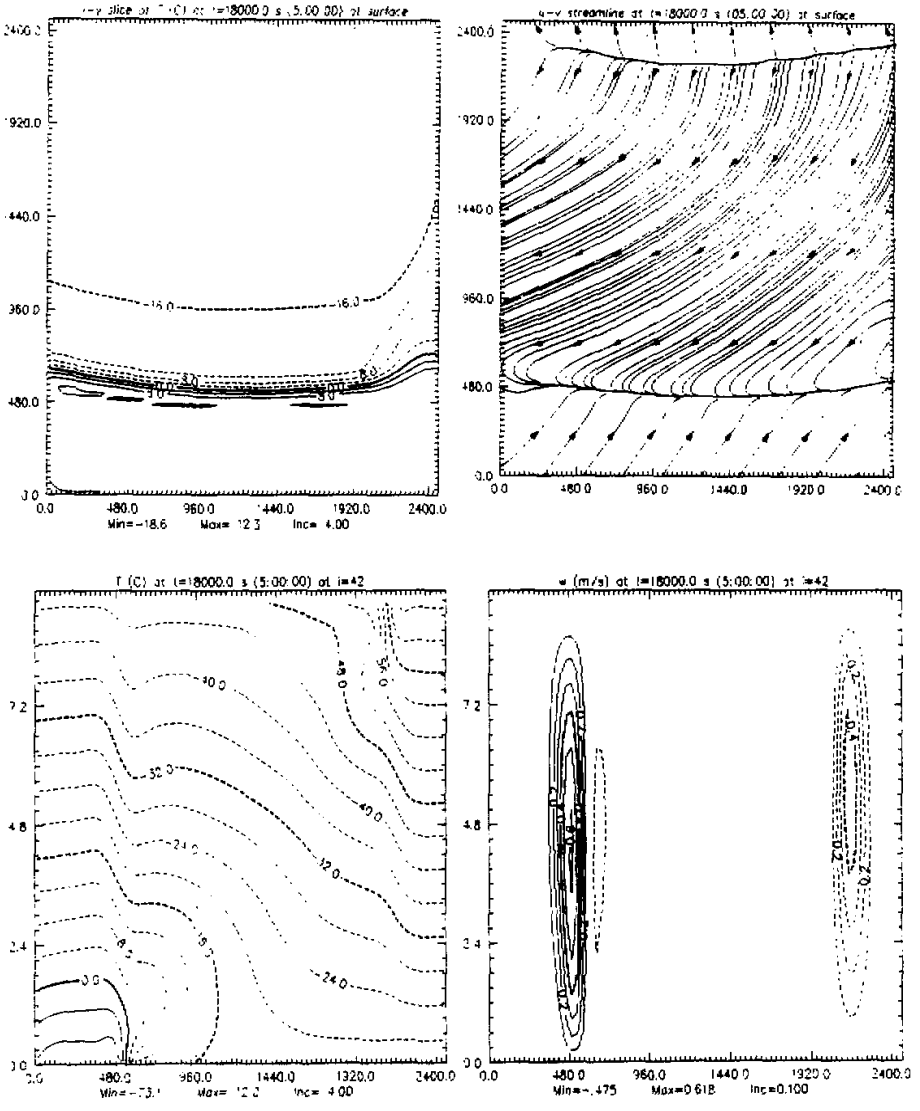

Fig. 2. The horizontal distributions at surface and the vertical distributions through the center in x direction in control experiment, at t = 5.0 h. (a) the horizontal distribution of temperature; (b) the horizontal distribution of u–v streamline; (c) the vertical distribution of temperature; (d) the vertical distribution of vertical velocity.

continually increase with the happening of the frontogenesis. Before and in the frontal area, the positive potential vorticity becomes larger, while the negative potential vorticity strengthens behind the frontal area. These changes are reasonable. In addition, the jet appears at both the top and bottom boundary respectively (figure not given). The result is also similar to that of Blumen and Wu (1995).

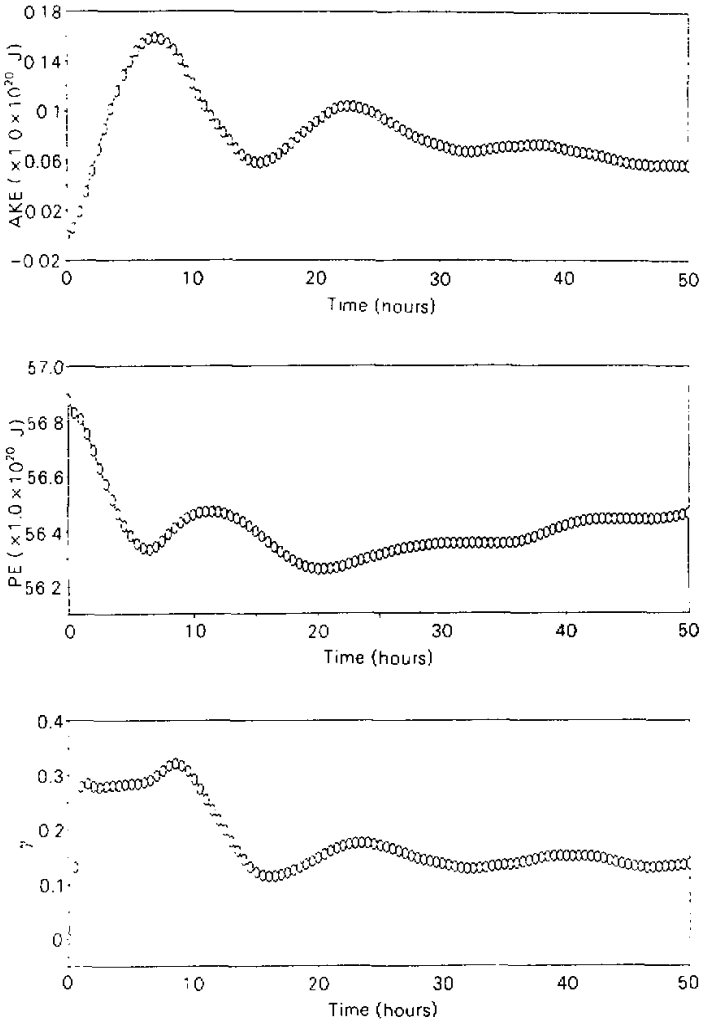

Fig. 3. The variation of energy with time during the evolution of the imbalanced flow in control experiment. (a) the variation of actual kinetic energy with time; (b) the variation of potential energy with time; (c) the variation of energy conversion ratio with time.

Fig. 3 represents the variation of the energy during the evolution.

Actual kinetic energy and potential energy are calculated by the following equations:

$$E_k = \int_\tau \frac{1}{2} \frac{p}{RT} (u^2 + v^2 + w^2) d\tau, \tag{13}$$

and

$$E_p = \int_\tau \frac{pgz}{RT} d\tau. \tag{14}$$

Where $d\tau = dxdydz$ denotes the volume element. From Fig. 3, it shows that during the evolution, both actual kinetic energy and potential energy periodically vary with an inertial oscillation. The oscillation period is about 17 hours, equivalent to $\frac{2\pi}{f}$. And the oscillation amplitude becomes smaller and smaller during the evolution. But the stationary balanced state can only be approached as it cannot be reached in the limit duration of time. The phase of actual kinetic energy is opposite to that of the potential energy. When the actual kinetic energy reaches its maximum, the potential energy reduces to its minimum and vice versa. Generally, when the potential energy is decreasing, the actual kinetic energy is increasing, and $\left|\frac{\partial\theta}{\partial y}\right|$ near the surface is increasing, that is to say, the frontogenesis occurs. While when the potential energy is increasing and the kinetic energy is decreasing, $\left|\frac{\partial\theta}{\partial y}\right|$ near the surface is decreasing, that is to say, the frontolysis occurs. So we can conclude that the energy conversion is bidirectional, the potential energy can be converted into the actual kinetic energy, which induces frontogenesis, and the actual kinetic energy can also be converted into the potential energy, which induces frontolysis. The inertial oscillation of the energy conversion leads to the inertial oscillation of the evolution of the front. From Fig. 3c, it shows that the energy conversion ratio also varies with an inertial oscillation at the Coriolis f. And the phase of the energy conversion ratio is identical to the phase of the actual kinetic energy. It varies in the range of [0, 1 / 3]. Its amplitude becomes smaller and smaller with time, and finally reaches a stable value. These results account for the situation about the three-dimensional fully compressible stratified fluid during the nonlinear evolution, which does not satisfy the conservation of the potential vorticity.

3.2 *With different initial temperature gradient*

What will happen if the initial temperature gradient is different from the control experiment? Fig. 4 shows the distributions of the fields at initial time or at $t = 5.0$ h.

Compared with the control experiment, the initial temperature gradient here is weaker and the isotherm is sparser. So that after nonlinear adjustment, the cold frontogenesis also occurs, but both its intensity (the denseness of the isotherm) and its movement are weaker than those of the control experiment. Fig. 4d shows that the final vertical velocity is also weaker than that of the control experiment for the weaker initial temperature gradient. The final potential vorticity in the frontal area is also weaker than that of the control experiment (figure not shown).

The variation of the actual kinetic energy and the potential energy during the evolution are given in Fig. 5.

Similar to the control experiment, the potential energy, the actual kinetic energy, and the energy conversion ratio all vary with an inertial oscillation. The amplitude is getting smaller during the evolution and finally close to a stable value, which shows that the stationary geostrophic balance can only be approached while cannot be reached. For the sake of the weaker initial temperature gradient, actual kinetic energy and potential energy here are much weaker than that of the control experiment during the evolution. Fig. 5c shows that the energy conversion ratio is also in the range of [0, 1 / 3]. And the final stable value is directly related to the initial temperature gradient. The stronger the initial temperature gradient is, the higher the final energy conversion ratio is.

3.3 *With vapor distribution*

For the evidently sea-land typed vapor distribution, the initial fields are shown in Fig. 6.

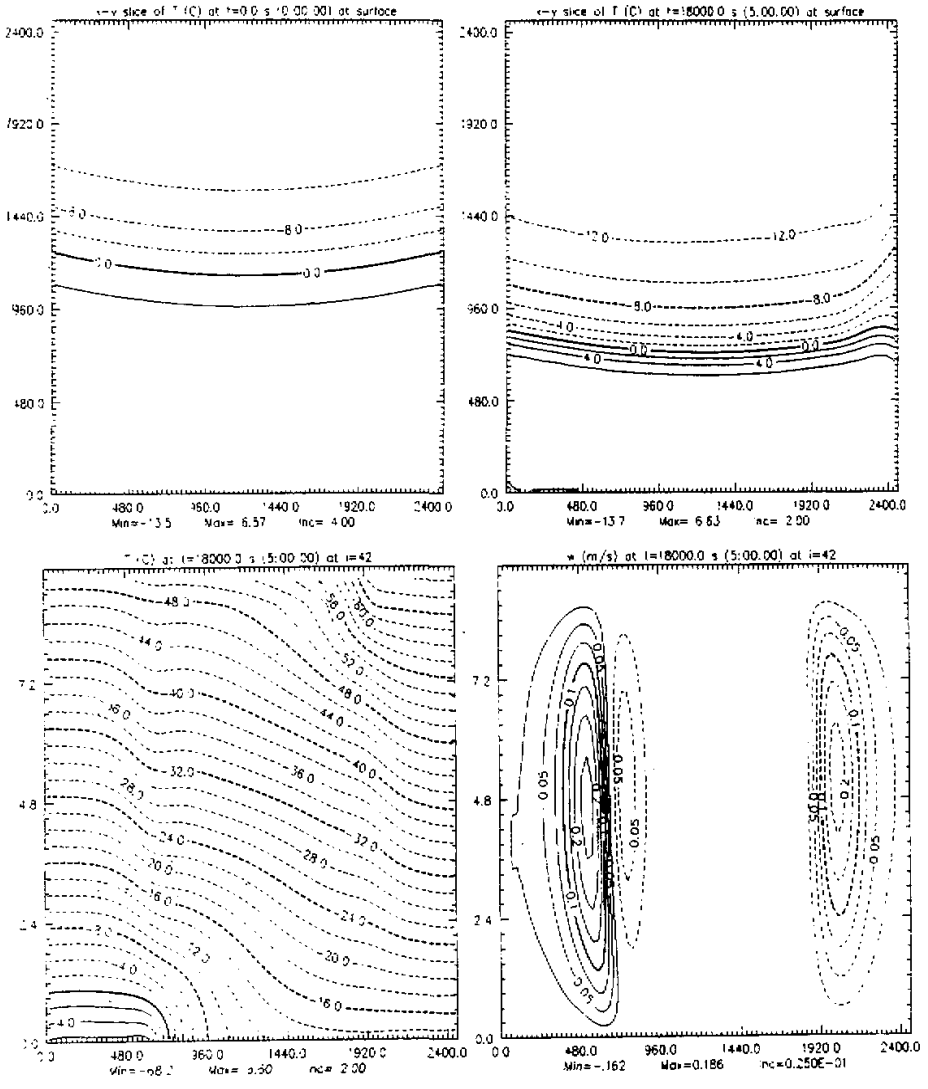

Fig. 4. The distributions of the intial fields and the distributions of the fields at $t = 5.0$ h with the weaker initial temperature gradient. (a) the initial horizontal temperature at surface; (b) at $t = 5.0$ h, the horizontal distribution of temperature; (c) at $t = 5.0$ h, the vertical distribution of temperature; (d) at $t = 5.0$ h, the vertical distribution of vertical velocity.

Figure 6 shows that the specific humidity is larger in the sea area, in the warm area and at low level than in the land area, in the cold area and at high level respectively. With this initial condition, the frontogenesis will be different from that of the control experiment during the evolution, as shown in Fig. 7.

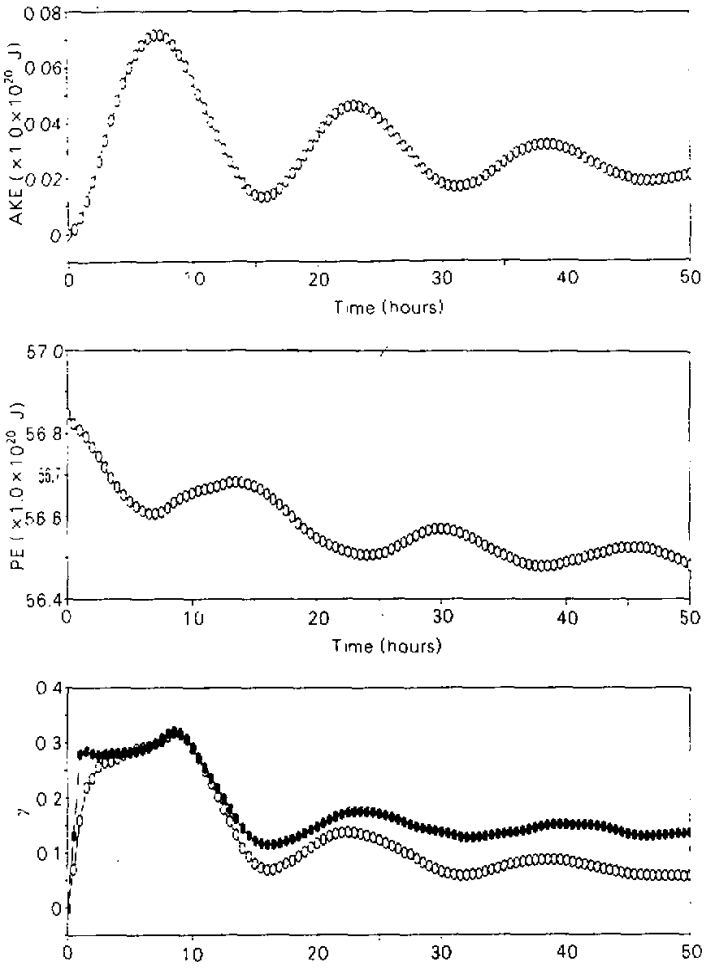

Fig. 5. The variation of energy with time during the evolution of the imbalanced flow with the weaker initial temperature gradient. (a) the variation of the actual kinetic energy with time; (b) the variation of potential energy with time; (c) the variation of the energy conversion ratio with time. (hollow points are with weaker initial temperature gradient, solid points are in control experiment)

Fig. 7 shows that owing to the participation of the vapor distribution, the intensified effects of $\partial\theta / \partial y$ in the sea area and in the land area are no longer uniform. In sea area, the latent energy is released due to condensation, which makes $\partial\theta / \partial y$ stronger and brings forward the time of the frontogenesis; while in land area, no latent energy is released, the intensified effect on $\partial\theta / \partial y$ is weaker, and the time for $\partial\theta / \partial y$ to reach a certain value is longer. Fig. 7b is the distribution of surface streamline at $t=3.0$ h. Furthermore, it shows that in the eastern sea area, the surface convergence line moves south slower than that of in the western land area, then the front breaks into two parts during

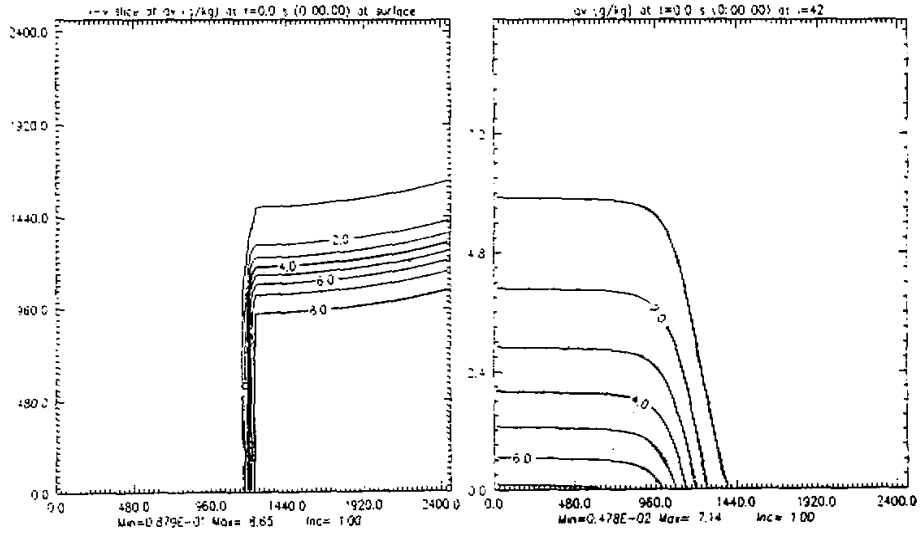

Fig. 6. The distribution of sea–land typed vapor field (a) the horizontal distribution of vapor at surface; (b) the vertical distribution of vapor (through the center in x direction).

the nonlinear evolution. Fig. 7c represents the distribution of surface temperature at $t=5.0$ h. Compared with the control experiment, the surface cold front is no longer unbent and the torsion is observed at the middle part. In the western land area, the denseness of the isotherm is the same as that of the control experiment, but in the eastern sea area, due to the participation of vapor distribution, the denseness of the isotherm is evidently greater, and the cold front is much stronger. Fig. 7d is the distribution of surface potential vorticity at $t=5.0$ h. It shows that the axis of surface potential vorticity also becomes torsional at the middle part. The value of the surface potential vorticity in sea area is evidently greater than that in land area. The increasing of the surface potential vorticity reveals the strengthening of the surface front to a certain extent. From the variation of the potential vorticity, we can conclude that the vapor distribution can influence the frontogenesis greatly.

Fig. 8a and Fig. 8b show that the same inertial oscillations also happen in the variations of the actual kinetic energy and the potential energy when there is vapor distribution in the initial fields. The oscillation frequency is also equal to f, and the amplitude is decreasing with time. Because the latent energy released during the condensation process is favorable for the frontogenesis, it will strengthen the conversion from potential energy to actual kinetic energy, and the final actual kinetic energy will be greater than that of the control experiment. Fig. 8c shows the variation of the energy conversion ratio with time. It also shows that the energy conversion ratio also varies in the same range as in the control experiment. However, the final value is greater than that of the control experiment due to the influence of the vapor distribution.

If the vapor distribution is strip–like type, either the intensity of the cold front or the final energy conversion ratio is larger than that in the control experiment. That is to say, it has greater influence on the frontogenesis. However, the similar inertial oscillations will occur in the evolution, and the range of the energy conversion ratio is also the same. Furthermore, compared with the above case that vapor distribution is sea–land type, the frontogenesis along the east–west direction in this case is uniform.

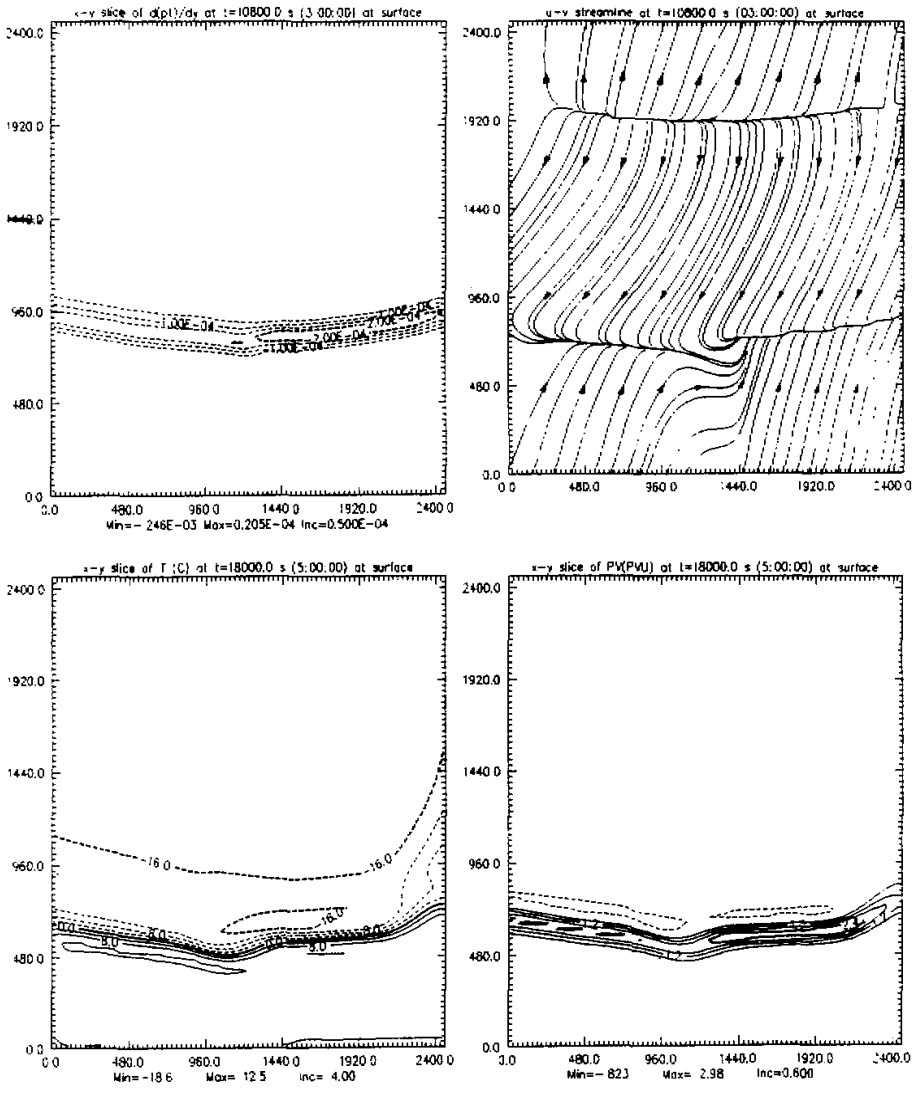

Fig. 7. The horizontal distributions of the fields during the evolution of the imbalanced flow with sea-land typed vapor distribution. (a) at $t=3.0$ h, the horizontal distribution of $\partial\theta / \partial y$ at surface; (b) at $t=3.0$ h, the horizontal distribution of u-v streamline at surface; (c) at $t=5.0$ h, the horizontal distribution of temperature at surface; (d) at $t=5.0$ h, the horizontal distribution of potential vorticity at surface.

And the movement of the eastern part is as fast as that of the western part. All figures in this case are not given for simplicity.

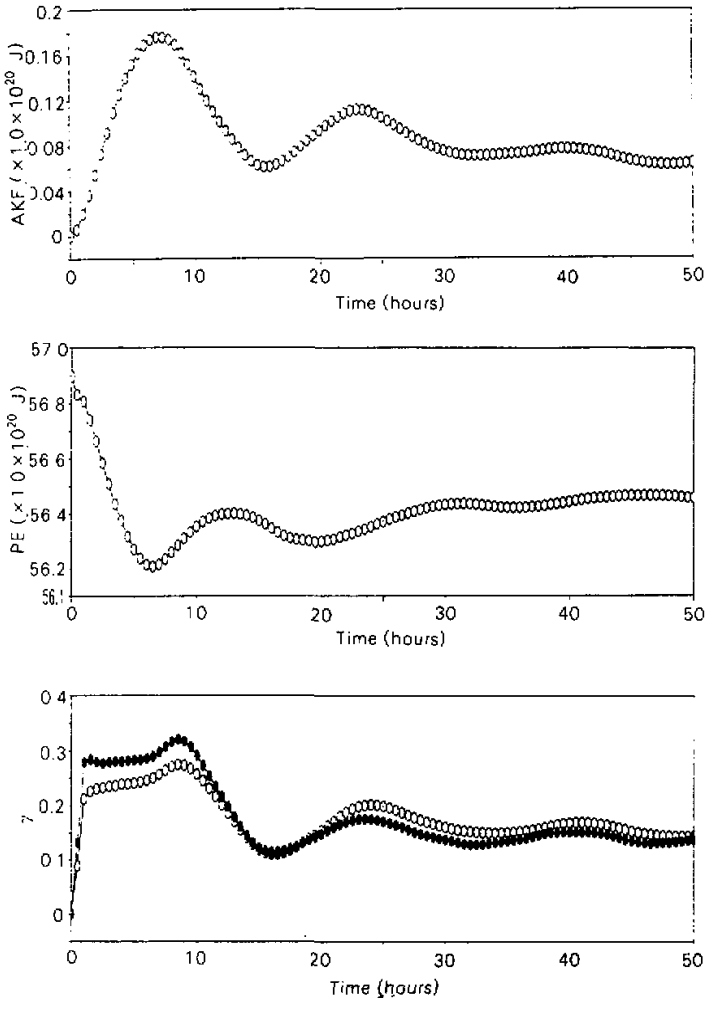

Fig. 8. The variation of energy with time during the evolution of the imbalanced flow with sea–land typed vapor distribution. (a) the variation of actual kinetic energy with time; (b) the variation of potential energy with time; (c) the variation of energy conversion ratio with time. (hollow points are with vapor distribution; solid points are in control experiment)

3.4 *With orographic effect*

When there is a mountain in the center of the domain, the temperature distributions during the evolution are given as shown in Fig. 9 and Fig. 10, at times: $t=0.0$ h, $t=2.0$ h, $t=3.5$ h, and $t=5.0$ h.

It can be found that the cold front is gradually forming and moving down-slope with its intensity increasing. The cold front becomes torsional due to the influence of the mountain. The eastern part of the cold front moves faster than the western part, so that the part of the cold front near the mountain is finally along southeast–northwest direction.

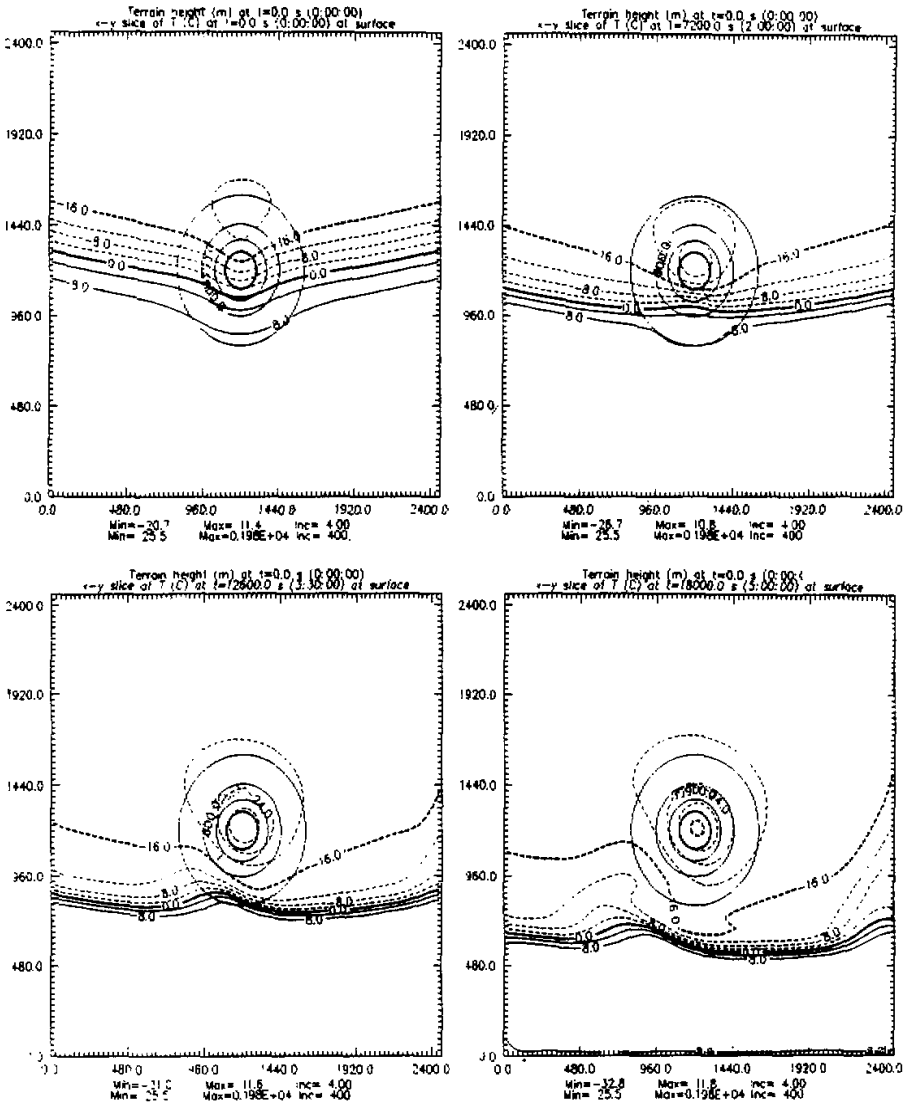

Fig. 9. The surface temperature distributions during the evolution of the unbalanced flow (the homocentric circles denote terrain) with orographic forcing. (a) at $t=0.0$ h, the distribution of surface temperature; (b) at $t=2.0$ h, the distribution of surface temperature; (c) at $t=3.5$ h, the distribution of surface temperature; (d) at $t=5.0$ h, the distribution of surface temperature.

Fig. 11 is the vertical distributions of vorticity and divergence at times: $t=0.5$ h and $t=5.0$ h.

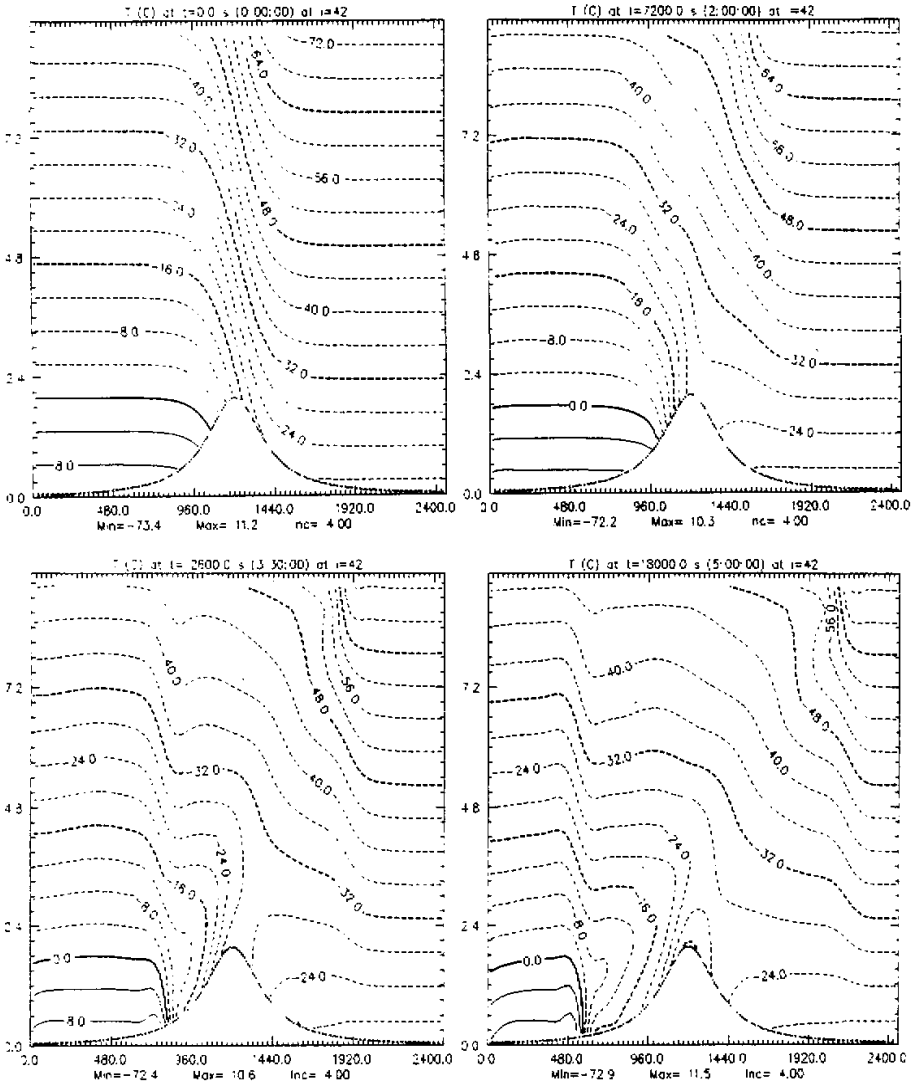

Fig. 10. The vertical distributions of temperature during the evolution of the unbalanced flow with orographic forcing. (a) at $t=0.0$ h, the vertical distribution of temperature; (b) at $t=2.0$ h, the vertical distribution of temperature; (c) at $t=3.5$ h, the vertical distribution of temperature; (d) at $t=5.0$ h, the vertical distribution of temperature.

Fig. 11a and Fig. 11b show that: before the cold front, the positive vorticity center is at low level and the negative vorticity center is at high level; behind the cold front, the positive vorticity center is at high level and the negative vorticity center is at low level. During the evolution, the vorticity centers at low level are moving south with the cold front, while the vorticity centers at high level are moving

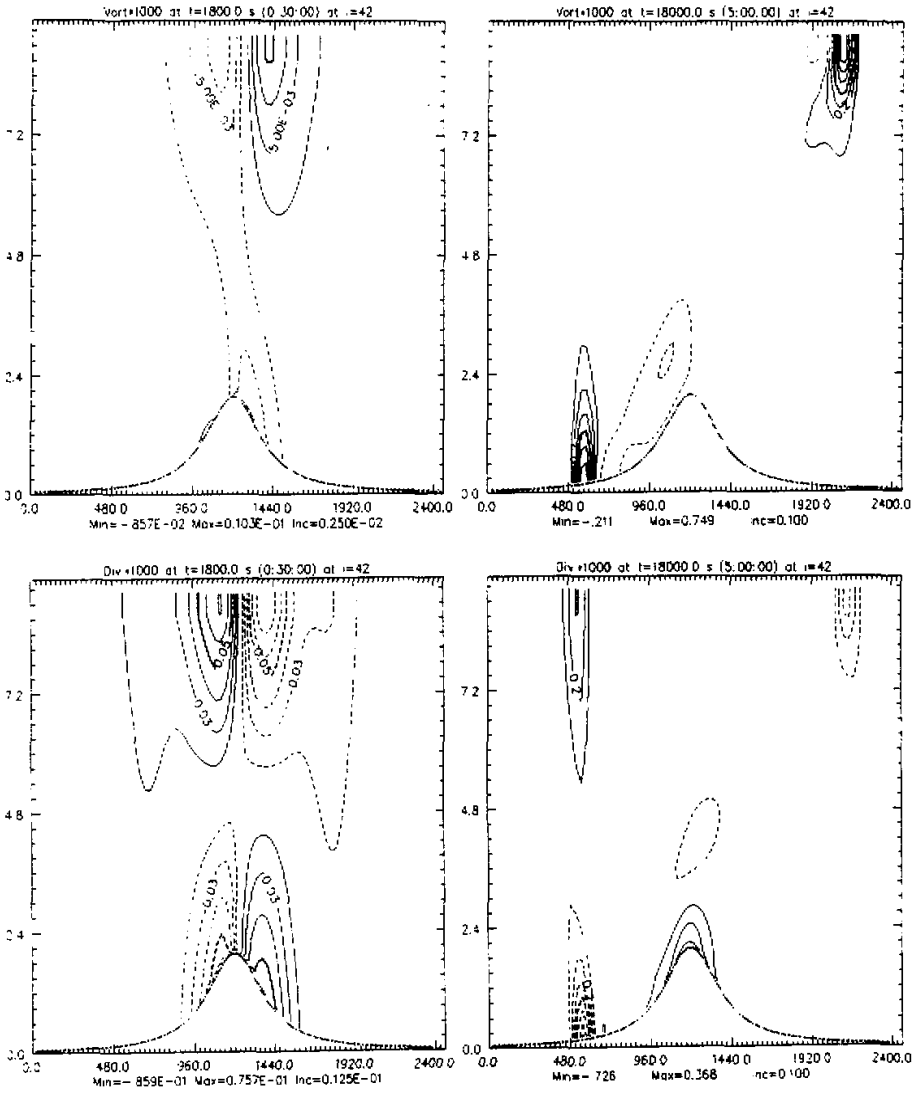

Fig. 11. The vertical distributions of vorticity and divergence during the evolution of the unbalanced flow with orographic forcing. (a) at $t=0.5$ h, the vertical distribution of vorticity; (b) at $t=5.0$ h, the vertical distribution of vorticity; (c) at $t=0.5$ h, the vertical distribution of divergence; (d) at $t=5.0$ h, the vertical distribution of divergence.

north. When the negative vorticity center at high level overlaps the positive vorticity center at low level, the interaction of vorticity at different levels would enhance and accelerate the cold surface frontogenesis. Figures 11c and 11d show that the convergence area at low level and the divergence area at high level before the surface cold front are moving south with the cold front. The divergence

center at low level behind the surface cold front always remains at the peak of the mountain, which may be induced by the influence of the mountain.

The influence of the mountain can also be found in the variation of the energy. Figure 12 is the variation of the actual kinetic energy, the potential energy and the energy conversion ratio.

It also shows that there are similar inertial oscillations in the evolution with a mountain at the center of the domain. The oscillation frequency is also equal to f, and the amplitude is decreasing with time. The energy conversion ratio also varies in the range of [0, 1 / 3]. When the cold front is moving down-slope, the orographic forcing is favorable for the energy conversion from potential energy to

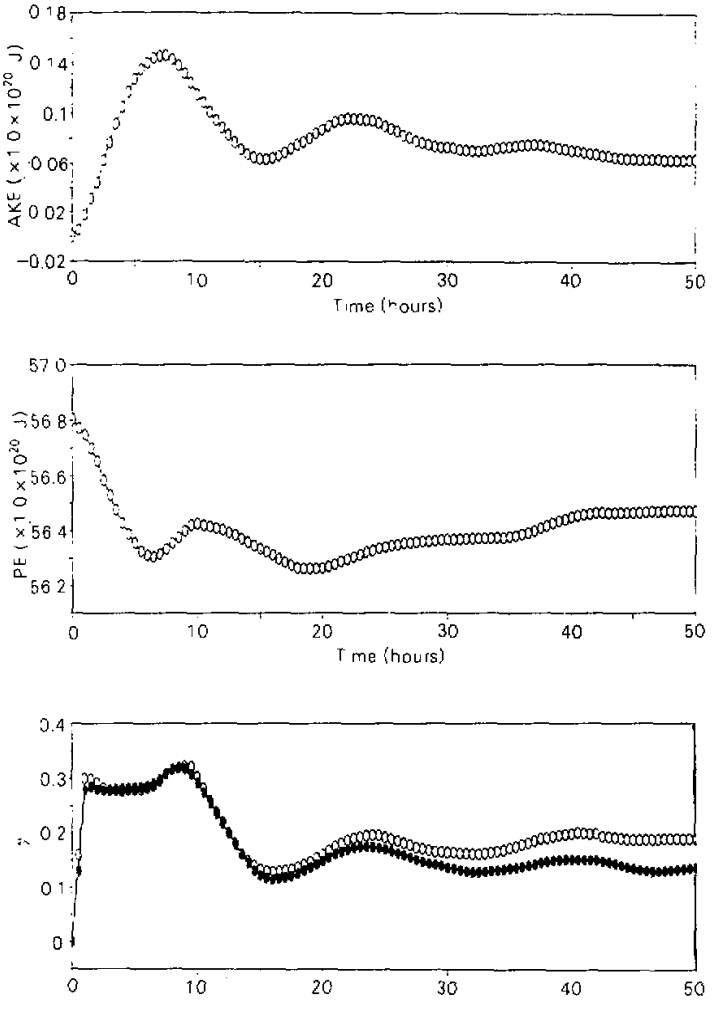

Fig. 12. The variation of energy with time during the evolution of the imbalanced flow with orographic forcing. (a) the variation of actual kinetic energy with time; (b) the variation of potential energy with time; (c) the variation of energy coversion ratio with time. (hollow points are with orographic forcing, solid points are in control experiment)

the actual kinetic energy, so that the final actual kinetic energy and the final energy conversion ratio are also greater than those of the control experiment.

Changing the mountain, promising that the cold frontogenesis will occur and be kept at the up–slope side, we can also find that there are inertial oscillations happening in the evolution and the range of the energy conversion ratio is the same as that in the control experiment. In this case the influence of the orographic forcing is not favorable for the energy conversion, the final energy conversion ratio and the actual kinetic energy are weaker than those of the control experiment (figures not shown).

4. Conclusions

In this paper, a three–dimensional non–hydrostatic fully compressible meso–scale model (ARPS) is used to study the evolution of the stratified fluid when its initial fields are not in geostrophic balance. Four cases are designed and compared: (i) control experiment; (ii) with different initial temperature gradient; (iii) with vapor distribution; (iv) with orographic forcing. Our numerical results show that:

(1) There is an inertial oscillation in the evolution of the imbalanced flow with the frequency f, and its amplitude is decreasing with time. The stationary balanced state can only be approached while cannot be reached in the limit duration of time. The energy conversion is bidirectional: potential energy can be converted into the kinetic energy and the kinetic energy can also be converted into the potential energy, which are in a balanced evolving state. The energy conversion ratio also varies with an inertial oscillation. And the range of the energy conversion ratio is $[0, 1/3]$;

(2) The initial temperature gradient can greatly influence the cold frontogenesis during the evolution. The stronger the initial temperature gradient is, the stronger the cold front will be the stronger the final actual kinetic energy will be, and the higher the final energy conversion ratio will be and vice versa;

(3) Suitable vapor distribution is evidently favorable for the cold frontogenesis. It will accelerate the frontogenesis, influence the shape of the cold, strengthen the intensity of the cold front, and influence the final energy conversion ratio. The larger area of vapor distribution and the higher relative humidity will have greater influence on the frontogenesis. The sea–land typed vapor distribution can make the frontogenesis in sea area stronger than the frontogenesis in land area. There are also inertial oscillations in the evolution with vapor distribution, and the energy conversion ratio will become greater due to the participation of vapor distribution;

(4) The orographic forcing has an evidently strengthening effect on the frontogenesis. The effect on the frontogenesis and the influence on the final energy conversion ratio depend on the relative location of the mountain to the cold front. The inertial oscillation also happens in the nonlinear evolution. The orographic forcing can greatly influence the energy conversion ratio: if the cold front is formed at the down–slope, the orographic forcing will be favorable for the energy conversion ratio. Otherwise, if the cold front is formed at the up–slope, the orographic forcing will be of disadvantage to the energy conversion ratio. The final energy conversion ratio will change with the influence of the orographic forcing.

REFERENCES

Blumen, W., 1972: Geostrophic adjustment. *Rev. Geophys. Space Phys.*, **10**, 485–528.

——, and R. Wu, 1995: Geostrophic adjustment: Frontogenesis and energy conversion. *J. Phys. Oceanogr.*, **25**, 428–438.

——, 2000: Inertial Oscillation and frontogenesis in a zero potential vorticity model. *J. Phys. Oceanogr.*, **30**, 31–39.

Boss, E., and L. Thompson., 1985: Energetics of nonlinear geostrophic adjustment. *J. Phys. Oceanogr.*, **25**, 1521–1529.

Gill, A.E., 1976: Adjustment under gravity in a rotating channel. *J. Fluid. Mech.*, **77**, 603–621.

——, 1982: *Atmosphere—Ocean Dynamics*, Academic Press, 662 pp.

Glendening, J. W., 1993: Nonlinear displacement of the geostrophic velocity jet created by mass imbalance. *J. Atmos. Sci.*, **50**, 1617–1628.

Grimshaw, R. H. J., et al., 1998: Energetics of linear geostrophic adjustment in stratified rotating fluids. *J. Mar. Res.*, **56**, 1203–1224.

Majid M. F., and R. Wu, 1998: A numerical study of geostrophic adjustment and frontogenesis. *Acta. Meteor. Sinica.*, **15**, 179–192.

McWilliams, J. C., 1988: Vortex generation through balanced adjustment. *J. Phys. Oceanogr.*, **18**, 1178–1192.

Middleton, J. F., 1987: Energetics of linear geostrophic adjustment. *J. Phys. Oceanogr.*, **17**, 735–740.

Ming Xue et al., 1995: *ARPS Version 4.0 User's Guide*, Center for Analysis and Prediction of Storm, 380pp.

Ou, H. W., 1984: Geostrophic adjustment: A mechanism for frontogenesis. *J. Phys. Oceanogr.*, **14**, 994–1000.

——, 1986: On the energy conversion during geostrophic adjustment. *J. Phys. Oceanogr.*, **16**, 2203–2204.

Rossby, C.–G., 1938: On the mutual adjustment of pressure and velocity distribution in simple current systems, II. *J. Mar. Res.*, **1**, 239–263.

Van Heijst, G.J.F., 1985: A geostrophic adjustment model of a tidal mixing front. *J. Phys. Oceanogr.*, **15**, 1182–1190.

Wang, Y., and R. Wu., 1998: The influence of stratification on frontogenesis caused by geostrophic adjustment. *Acta. Meteor. Sinica.*, **12**, 376–381.

Wu, R., and W. Blumen., 1995: Geostrophic adjustment of a zero potential vorticity flow initiated by a mass imbalance. *J. Phys. Oceanogr.*, **25**, 439–445.